

Formation rate of gravitational structures and the cosmic X-ray background radiation

Tetsu Kitayama^{*} and Yasushi Suto[†]

Department of Physics, The University of Tokyo, Bunkyo-ku, Tokyo 113, Japan

Accepted 1995 November 27

ABSTRACT

Analytical expressions for the rates of formation and destruction of gravitationally bound systems are derived assuming that they are originated from primordial random-Gaussian density fluctuations. The resulting formulae reproduce the time derivative of the Press-Schechter mass function in a certain limit. Combining a theoretical model for the evolution of structures with the formation rate, we can make various cosmological predictions which are to be compared with observations. As an example to elucidate such applicability, we evaluate the contribution of clusters of galaxies to the cosmic X-ray background radiation. With the *COBE* normalization, we find that the significant fraction of the observed soft X-ray background is accounted for by clusters of galaxies in a cold dark matter universe with $\Omega_0 \sim 0.2$, $\lambda_0 = 1 - \Omega_0$ and $h \sim 0.8$.

Key words: cosmology: theory - dark matter - clusters: formation - clusters: evolution - X-rays: sources.

1 INTRODUCTION

Formation, merging, and destruction history of dark matter haloes of astrophysical objects is of fundamental importance in describing the subsequent formation and evolution of luminous objects such as quasars, galaxies, and clusters of galaxies. In addition, early formation of structures may affect the growth of objects through the reionization of the entire universe (Sasaki, Takahara, & Suto 1993; Sasaki & Takahara 1994; Fukugita & Kawasaki 1994).

Key quantities in this context are the rates of formation and destruction of gravitationally bound systems. They are defined as the comoving number density of bound systems of a given mass that are formed or destroyed in unit time at a given epoch. A number of authors have attempted to compute this quantity either numerically or analytically. A straightforward approach is to use a state-of-art numerical simulations (e.g., Evrard 1990; Cen & Ostriker 1992; Bryan et al. 1994; Sugihara 1994). Although the dynamical range and small-scale resolution of available codes are rapidly increasing, it is not clear at present to what extent they unambiguously describe small-scale dynamics. Besides it is not easy to grasp the underlying key physics from the results of

numerical simulations. It is therefore important to develop an analytical model on the basis of simple physics.

The alternative approach in such a direction is closely related to the theory of Press & Schechter (1974; hereafter PS). PS derived a mass function, the number density as a function of mass and epoch, of virialized systems. The PS mass function, however, is not directly related to the rate of formation mentioned above. In fact, the time derivative of the PS mass function can become either positive or negative. Thus it can not be simply interpreted as the rate of formation, but rather corresponds to the balance between the rates of formation and destruction (Cavaliere, Colafrancesco & Scaramella 1991; Blain & Longair 1993a,b). Although several authors have adopted the time derivative of the PS mass function to approximate the formation rate of bound systems (e.g., Efstathiou & Rees 1988; Fukugita & Kawasaki 1994), its validity should be examined carefully. Blain & Longair (1993a,b) and Sasaki (1994) correctly realized the above problem, and attempted to obtain the rates of formation and destruction separately, assuming some empirical forms for the rates. In this paper, we derive a more general formula for each rate on the basis of merger probabilities discussed by Bower (1991) and Lacey & Cole (1993; hereafter LC) (See also Kauffmann & White 1993).

Our formalism is applicable to a number of problems regarding the hierarchical clustering in the universe. In what follows we further apply the resultant formulae to the formation of clusters of galaxies and calculate their contribution to

^{*} e-mail: kitayama@utaphp1.phys.s.u-tokyo.ac.jp

[†] e-mail: suto@phys.s.u-tokyo.ac.jp, also at Research Center for the Early Universe, School of Science, The University of Tokyo, Bunkyo-ku, Tokyo 113, Japan

the observed cosmic X-ray background (XRB). The cluster contribution is in general supposed to be very small in the high energy band above a few keV, while it is likely to dominate in the soft energy band (Silk & Tarter 1973; Schaeffer & Silk 1988). It is, however, still uncertain to what extent the observed XRB can be contributed by emissions from clusters of galaxies. Several authors have employed the PS mass function to evaluate the cluster contribution (Evrard & Henry 1991; Blanchard et al. 1992; Burg, Cavaliere & Menci 1993), and thus formation epochs and the subsequent evolution of virialized clusters are not well specified in their treatment. Here we present an approach which explicitly takes account of the formation epoch of clusters and their luminosity evolution. Our predictions are made specifically in cold dark matter (CDM) universes with/without the cosmological constant whose fluctuation spectra are properly normalized by the *COBE* data (Sugiyama 1995). The results are also compared with those of the hydrodynamical simulation and the *ASCA* observations.

The plan of this paper is as follows. In Section 2, we outline the PS formalism and discuss how the time derivative of its mass function is related to the formation and destruction rates of bound systems. Then using the merger probabilities of virialized haloes deduced by Bower (1991) and LC, we derive expressions for the rates of formation and destruction. These expressions are further employed to describe the distribution of formation epoch of bound systems. In Section 3, we apply our formulae and calculate the contribution of clusters of galaxies to the XRB. Finally Section 4 is devoted to our conclusions and further discussion.

2 FORMATION AND DESTRUCTION RATES OF VIRIALIZED OBJECTS

2.1 Press-Schechter mass function

According to the hierarchical clustering model, small density fluctuations in the early universe grow via gravitational instability, become nonlinear, and eventually collapse to form bound virialized systems. For random Gaussian initial density fluctuations, the comoving number density of spherical collapsed systems in the mass range $M \sim M + dM$ at time t is evaluated as (Press & Schechter 1974; Bond et al. 1991)

$$N_{\text{PS}}(M, t) dM = \sqrt{\frac{2}{\pi}} \frac{\rho_0}{M} \frac{\delta_c(t)}{\sigma^2(M)} \left| \frac{d\sigma(M)}{dM} \right| \exp \left[-\frac{\delta_c^2(t)}{2\sigma^2(M)} \right] dM, \quad (1)$$

where ρ_0 is the mean comoving density of the universe, $\delta_c(t)$ is the critical density threshold for a spherical perturbation to collapse by the time t , and $\sigma(M)$ is the rms density fluctuation smoothed over a region of mass M . The latter two quantities are expressed respectively as

$$\delta_c(t) \equiv \frac{D(t_0)}{D(t)} \delta_c = \frac{\delta_c}{D(t)} \quad (\delta_c \simeq 1.69 \text{ for } \Omega_0 = 1), \quad (2)$$

and

$$\sigma^2(M) \equiv \sigma^2(M, t_0) = \frac{1}{(2\pi)^3} \int P(k, t_0) \hat{W}_M^2(k) d^3k, \quad (3)$$

where $D(t)$ is the linear growth factor normalized to unity at the present epoch t_0 , Ω_0 is the cosmological density parameter, $P(k, t_0)$ is the present power spectrum of density

fluctuations, and $\hat{W}_M(k)$ is the Fourier transform of a real space window function whose volume contains mass M .

Let us now consider the time derivative of the PS mass function (1):

$$R_{\text{PS}}(M, t) \equiv \frac{dN_{\text{PS}}(M, t)}{dt} = \left[\frac{\delta_c(t)}{\sigma^2(M)} - \frac{1}{\delta_c(t)} \right] \left[-\frac{d\delta_c(t)}{dt} \right] N_{\text{PS}}(M, t). \quad (4)$$

The above expression is positive only for $\sigma(M) < \delta_c(t)$ since $d\delta_c(t)/dt < 0$. This implies that $R_{\text{PS}}(M, t)$ is negative for low-mass objects for almost all realistic power spectra and window functions. Consider for instance scale-free spectra $P(k) \propto k^n$, which yield $\sigma^2(M) \propto M^{-(n+3)/3}$ where $n \gtrsim -3$ is physically plausible. The r.h.s. of equation (4) becomes negative for $M < M_c(t)$ where $M_c(t)$ is the critical mass at which $\sigma(M) = \delta_c(t)$. This clearly indicates that $R_{\text{PS}}(M, t)$ should not be interpreted as the formation rate of bound objects. Rather it corresponds to the net rate of change in the number density. In other words, $R_{\text{PS}}(M, t)$ consists of the formation rate $R_{\text{form}}(M, t)$ at which objects of a given mass M are formed by mergers of smaller mass objects, and the destruction rate $R_{\text{dest}}(M, t)$ at which they are destroyed by coalescence to produce more massive systems. Thus equation (4) should formally be written as

$$R_{\text{PS}}(M, t) \equiv R_{\text{form}}(M, t) - R_{\text{dest}}(M, t), \quad (5)$$

(Cavaliere et al. 1991; Blain & Longair 1993a,b). The negative $R_{\text{PS}}(M, t)$ at $M < M_c(t)$ is then ascribed to an excess of the destruction rate over the formation rate in this mass range. On the other hand, the formation rate dominates at $M > M_c(t)$ resulting in the positive $R_{\text{PS}}(M, t)$. In the case of scale-free spectra with $n > -3$, the critical mass $M_c(t)$ increases monotonically with time because $M_c(t) \propto D(t)^{6/(n+3)}$. This is a generic feature in the ‘bottom-up picture’ of hierarchical structure formation, in which small-scale structures form first and large-scale structures appear later. Our main task in this paper is to derive analytical expressions for $R_{\text{form}}(M, t)$ and $R_{\text{dest}}(M, t)$. In so doing, we find that a more specific definition of formation and destruction is essential in separating properly the two terms in equation (5).

2.2 Conditional probabilities of merger process

Merging is one of the most fundamental physical processes for the formation and destruction of virialized systems. LC developed a method to treat this process analytically following the idea of Bond et al. (1991). Their results are strictly justified only when one adopts the sharp k -space filtering, i.e. the spherical top-hat filtering in k -space, and when $\sigma(M)$ is a monotonically decreasing function of M . They found an analytical expression for the conditional probability that a point in a universe resides in an object of mass $M_1 \sim M_1 + dM_1$ at time t_1 provided it becomes part of a larger object of mass $M_2 (> M_1)$ at later time $t_2 (> t_1)$:

$$P_1(M_1, t_1 | M_2, t_2) dM_1 = \frac{1}{\sqrt{2\pi}} \frac{\delta_{c1} - \delta_{c2}}{(\sigma_1^2 - \sigma_2^2)^{3/2}} \left| \frac{d\sigma_1^2}{dM_1} \right| \exp \left[-\frac{(\delta_{c1} - \delta_{c2})^2}{2(\sigma_1^2 - \sigma_2^2)} \right] dM_1, \quad (6)$$

where $\sigma_i \equiv \sigma(M_i)$ and $\delta_{ci} \equiv \delta_c(t_i)$ for $i = 1$ and 2 . The same expression was obtained in a more heuristic manner by Bower (1991). The reverse conditional probability that a point resides in an object of mass $M_2 \sim M_2 + dM_2$ at time t_2 provided it has been part of a smaller object of mass $M_1 (< M_2)$ at $t_1 (< t_2)$ is

$$P_2(M_2, t_2 | M_1, t_1) dM_2 = \frac{1}{\sqrt{2\pi}} \frac{\delta_{c2}(\delta_{c1} - \delta_{c2})}{\delta_{c1}} \left[\frac{\sigma_1^2}{\sigma_2^2(\sigma_1^2 - \sigma_2^2)} \right]^{\frac{3}{2}} \left| \frac{d\sigma_2^2}{dM_2} \right| \times \exp \left[-\frac{(\sigma_2^2 \delta_{c1} - \sigma_1^2 \delta_{c2})^2}{2\sigma_1^2 \sigma_2^2 (\sigma_1^2 - \sigma_2^2)} \right] dM_2. \quad (7)$$

Equations (6) and (7) readily yield instantaneous transition rates from a certain mass to another. Setting $t_1 = t - \Delta t$, $t_2 = t$ and $M_2 = M$ in equation (6), and taking the limit $\Delta t \rightarrow 0$, one obtains

$$\frac{dP_1(M_1 \rightarrow M; t)}{dt} dM_1 \equiv \lim_{\Delta t \rightarrow 0} \frac{P_1(M_1, t - \Delta t | M, t)}{\Delta t} dM_1 = \frac{1}{\sqrt{2\pi}} \frac{1}{(\sigma_1^2 - \sigma^2)^{3/2}} \left[-\frac{d\delta_c(t)}{dt} \right] \left| \frac{d\sigma_1^2}{dM_1} \right| dM_1. \quad (8)$$

This quantity is interpreted as the rate at which an object of mass $M (> M_1)$ is formed from an object of mass $M_1 \sim M_1 + dM_1$ in unit time at t . Similarly from equation (7), one finds

$$\frac{dP_2(M \rightarrow M_2; t)}{dt} dM_2 \equiv \lim_{\Delta t \rightarrow 0} \frac{P_2(M_2, t + \Delta t | M, t)}{\Delta t} dM_2 = \frac{1}{\sqrt{2\pi}} \left[\frac{\sigma^2}{\sigma_2^2(\sigma^2 - \sigma_2^2)} \right]^{\frac{3}{2}} \left[-\frac{d\delta_c(t)}{dt} \right] \left| \frac{d\sigma_2^2}{dM_2} \right| \times \exp \left[-\frac{(\sigma^2 - \sigma_2^2) \delta_c^2(t)}{2\sigma^2 \sigma_2^2} \right] dM_2. \quad (9)$$

Equation (9) corresponds to the rate at which an object of mass $M (< M_2)$ is incorporated into a larger object of mass $M_2 \sim M_2 + dM_2$ at time t .

2.3 Formal procedure

Now we can write down the rates of formation and destruction of gravitationally bound systems using the transition rates in the last subsection. From equation (8), one *formally* defines the formation rate of an object of mass M at time t as

$$R_{\text{form}}(M, t) \equiv \int_0^M dM_1 \frac{dP_1(M_1 \rightarrow M; t)}{dt} N_{\text{PS}}(M, t) = \left[\frac{1}{\sqrt{\pi}} \frac{\delta_c(t)}{\sigma^2(M)} \int_0^\infty \frac{dx}{x^2} \right] \left[-\frac{d\delta_c(t)}{dt} \right] N_{\text{PS}}(M, t). \quad (10)$$

Equation (9) similarly defines the *formal* destruction rate:

$$R_{\text{dest}}(M, t) \equiv \int_M^\infty dM_2 \frac{dP_2(M \rightarrow M_2; t)}{dt} N_{\text{PS}}(M, t) = \left[\frac{1}{\delta_c(t)} + \frac{1}{\sqrt{\pi}} \frac{\delta_c(t)}{\sigma^2(M)} \int_0^\infty \frac{e^{-y^2}}{y^2} dy \right] \times \left[-\frac{d\delta_c(t)}{dt} \right] N_{\text{PS}}(M, t). \quad (11)$$

Clearly these formal expressions diverge, reflecting the divergence of equations (8) and (9) in the limit $M_1 \rightarrow M$ and

$M_2 \rightarrow M$, respectively. Such a divergence would simply be related to the fact that the above formalism identifies the formation and destruction of objects even if the associate change of mass is infinitesimal. In reality, however, such a small change in mass hardly corresponds to the formation or destruction in a usual sense; rather it should be regarded as accretion or evolution of the same system. In order to incorporate more realistic and physically reasonable description of these events, we should replace the above definitions of formation and destruction with more appropriate ones. Then the divergence associated in equations (10) and (11) would disappear naturally.

One may argue that the divergence is ascribed to counting the transition of a certain object to practically the *same* one, by showing explicitly that equations (10) and (11) diverge in a similar manner. In fact, one can prove that the divergences in the two rates exactly cancel out and their difference reduces to the time derivative of the PS mass function:

$$R_{\text{form}}(M, t) - R_{\text{dest}}(M, t) = \left[\frac{\delta_c(t)}{\sigma^2(M)} - \frac{1}{\delta_c(t)} \right] \left[-\frac{d\delta_c(t)}{dt} \right] N_{\text{PS}}(M, t) = R_{\text{PS}}(M, t). \quad (12)$$

The above result also suggests that the divergence in equations (10) and (11) can be removed by redefining the formation and destruction events properly. We will propose a realistic and reasonable prescription in the next subsection.

2.4 Realistic prescription to compute R_{form} and R_{dest}

Since the divergence mentioned in the last subsection is originated from counting the transitions from an object to the essentially *same* one, a simplest remedy is to introduce thresholds in the mass of formation and destruction events. More specifically, we replace equations (10) and (11) with

$$R_{\text{form}}(M, t; M_f) \equiv \int_0^{M_f} dM_1 \frac{dP_1(M_1 \rightarrow M; t)}{dt} N_{\text{PS}}(M, t), \quad (13)$$

and

$$R_{\text{dest}}(M, t; M_d) \equiv \int_{M_d}^\infty dM_2 \frac{dP_2(M \rightarrow M_2; t)}{dt} N_{\text{PS}}(M, t). \quad (14)$$

Physically the above procedure corresponds to assuming that an object of mass M keeps its identity as long as it stays between M_f and M_d , and to defining the formation and destruction of the object only when the associate mass change is out of this range. Adopting such a prescription, the above formulae are integrated to give

$$R_{\text{form}}(M, t; M_f) = \sqrt{\frac{2}{\pi}} \frac{1}{\sqrt{\sigma^2(M_f) - \sigma^2(M)}} \left[-\frac{d\delta_c(t)}{dt} \right] N_{\text{PS}}(M, t), \quad (15)$$

and

$$R_{\text{dest}}(M, t; M_d) = \left[\left(\frac{1}{\delta_c(t)} - \frac{\delta_c(t)}{\sigma^2(M)} \right) \text{erfc}(Z) + \frac{1}{\sqrt{\pi}} \frac{\delta_c(t)}{\sigma^2(M)} \frac{e^{-Z^2}}{Z} \right]$$

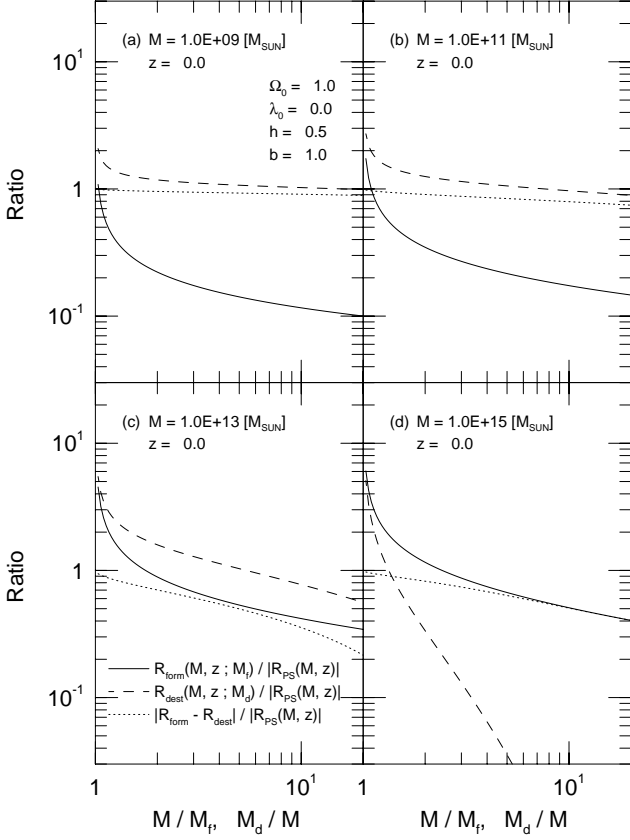


Figure 1. Dependence of $R_{\text{form}}(M, z; M_f)$ (solid curve), $R_{\text{dest}}(M, z; M_d)$ (dashed), and their difference (dotted) on M/M_f or M_d/M at $z = 0$ in the standard CDM model (each quantity is normalized by $|R_{\text{PS}}(M, z)|$); (a) $M = 10^9 M_\odot$, (b) $M = 10^{11} M_\odot$, (c) $M = 10^{13} M_\odot$, (d) $M = 10^{15} M_\odot$.

$$\times \left[-\frac{d\delta_c(t)}{dt} \right] N_{\text{PS}}(M, t), \quad (16)$$

where Z is defined as

$$Z(M, t; M_d) \equiv \delta_c(t) \sqrt{\frac{\sigma^2(M) - \sigma^2(M_d)}{2\sigma^2(M)\sigma^2(M_d)}}, \quad (17)$$

and $\text{erfc}(u)$ is the complimentary error function:

$$\text{erfc}(u) \equiv \frac{2}{\sqrt{\pi}} \int_u^\infty \exp(-t^2) dt. \quad (18)$$

In the above prescription, it is important to choose physically reasonable values for M_f and M_d . Admittedly it is inevitably artificial. We here propose to set $M_f = M/2$ and $M_d = 2M$ as in LC mainly because of the following two reasons. One is that the identity of an object of mass M is clearly retained between $M/2$ and $2M$. If a new object of mass M were formed from a parent object of mass greater than $M/2$, the parent object would make up the dominant part of the new object. Therefore such a process should correspond to *evolution* of the parent object rather than formation of a new object. The same is true for the destruction of an object of mass M which is incorporated into an object of mass less than $2M$.

The other reason is more practical; equations (15) and (16) are rather insensitive to the specific choice of M_f and

M_d at $M_f \approx M/2$ and $M_d \approx 2M$, and their difference agrees fairly well with $R_{\text{PS}}(M, t)$. To see such features more clearly, we plot $R_{\text{form}}(M, z; M_f)$, $R_{\text{dest}}(M, z; M_d)$ and their difference against M/M_f or M_d/M in Fig. 1 (each quantity is normalized by $|R_{\text{PS}}(M, z)|$). Hereafter in this paper, a CDM power spectrum of Davis et al. (1985) is adopted and the mass variance is evaluated by the following approximation (White & Frenk 1991):

$$\sigma \propto \left[1 - 0.4490(\Omega_0 h)^{0.1} \left(\frac{r_f}{h^{-1} \text{Mpc}} \right)^{0.1} + 0.6352(\Omega_0 h)^{0.2} \left(\frac{r_f}{h^{-1} \text{Mpc}} \right)^{0.2} \right]^{-10}, \quad (19)$$

where $h \equiv H_0/(100 \text{ km/sec/Mpc})$ is the dimensionless Hubble constant, and the top-hat filtering is implicitly assumed. The above approximation holds within 10% over the range $0.013(\Omega_0 h)^{-1} < r_f/(h^{-1} \text{Mpc}) < 10(\Omega_0 h)^{-1}$. Equation (19) is normalized by the relation $\sigma(r_f = 8h^{-1} \text{Mpc}) = b^{-1}$, where b is the biasing parameter. In this section, we present results only in the standard CDM model ($\Omega_0 = 1$, $h = 0.5$, and $b = 1$) for an illustrative purpose, while we consider other CDM variants (e.g., Table 1) in Section 3.

Panels (a)-(d) in Fig. 1 are plotted for several masses at present redshift $z = 0$. The figure shows that $R_{\text{form}}/|R_{\text{PS}}|$ and $R_{\text{dest}}/|R_{\text{PS}}|$ are fairly insensitive to M/M_f or M_d/M for $M/M_f, M_d/M \gtrsim 1.5$, and that $R_{\text{form}} - R_{\text{dest}} \approx R_{\text{PS}}$ within 30% for $M/M_f, M_d/M \lesssim 3$. Thus for practical purposes as well, the choice of $M_f = M/2$ and $M_d = 2M$ seems reasonable.

Figure 2 illustrates $R_{\text{form}}(M, z; M/2)$, $R_{\text{dest}}(M, z; 2M)$, their difference, and $|R_{\text{PS}}(M, z)|$ versus M in the standard CDM model. Both panels exhibit that $R_{\text{form}} < R_{\text{dest}}$ for small masses and $R_{\text{form}} > R_{\text{dest}}$ for large masses. The critical mass M_c at which $R_{\text{form}} = R_{\text{dest}}$ increases with time; $M_c \approx 10^{10} M_\odot$ at $z = 5$, and $M_c \approx 10^{14} M_\odot$ at $z = 0$ in this example. The difference between two rates is very close to R_{PS} except at $M \approx M_c$. The deviation simply arises from the fact that we set $M_f, M_d \neq M$, but is not important in practice because its amplitude is several orders of magnitude smaller than those of R_{form} and R_{dest} . With these results in mind, we adopt $M_f = M/2$ and $M_d = 2M$ in the rest of this paper, and simply use $R_{\text{form}}(M, t)$ and $R_{\text{dest}}(M, t)$ to denote $R_{\text{form}}(M, t; M/2)$ and $R_{\text{dest}}(M, t; 2M)$ respectively.

2.5 Formation epoch distribution

Before proceeding to the application of the results obtained in the previous subsections, let us discuss the formation epoch of virialized systems in some detail. First consider the probability that an object of mass M at time t_1 remains, without destructed, to have mass less than $2M$ at later time $t_2 (> t_1)$. We call this quantity *the survival probability*. It is evaluated by LC from equation (7) as

$$\begin{aligned} P_{\text{surv}}(M, t_1, t_2) &\equiv \int_M^{2M} P_2(M_2, t_2 | M, t_1) dM_2 \\ &= 1 - \frac{1}{2} \left[\frac{\delta_{c1} - 2\delta_{c2}}{\delta_{c1}} \right] \exp \left[\frac{2\delta_{c2}(\delta_{c1} - \delta_{c2})}{\sigma^2(M)} \right] \end{aligned}$$

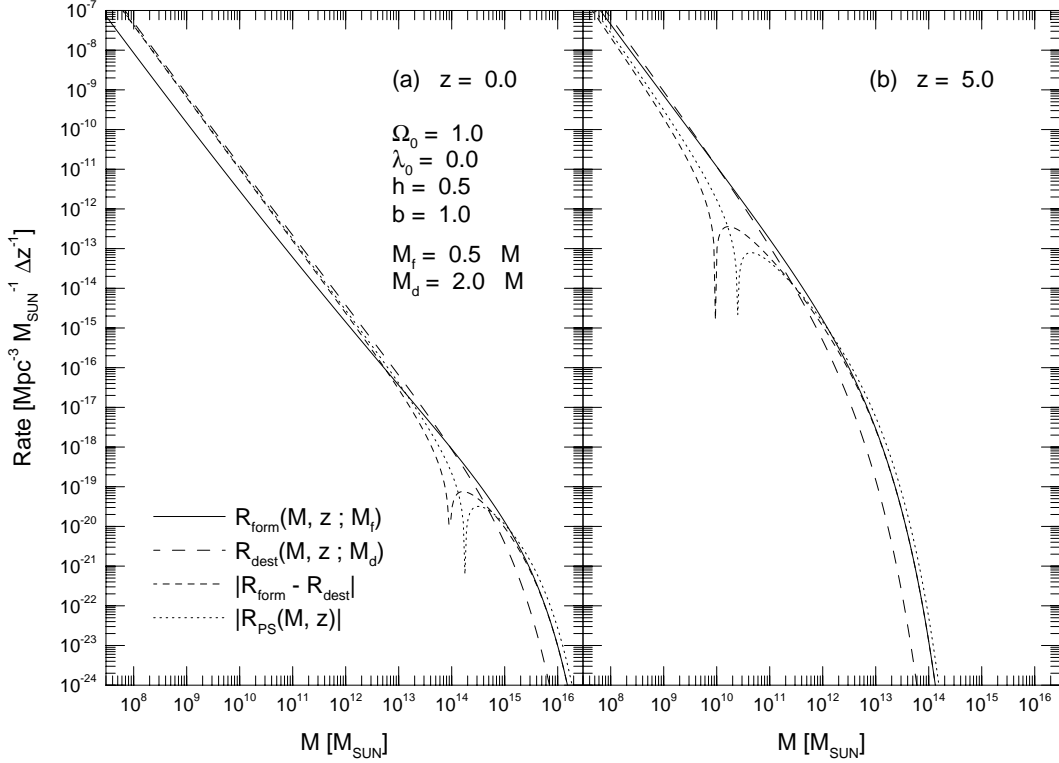


Figure 2. Rates of formation $R_{\text{form}}(M, z, M_f)$ (solid curve) and destruction $R_{\text{dest}}(M, z, M_d)$ (long-dashed) in the case of $M_f = M/2$ and $M_d = 2M$, as a function of mass in the standard CDM model. Also plotted are the absolute values of their difference (short-dashed) and $R_{\text{PS}}(M, z)$ (dotted); (a) $z = 0$, (b) $z = 5$.

$$\times \text{erfc}[X(M, t_1, t_2)] - \frac{1}{2} \text{erfc}[Y(M, t_1, t_2)], \quad (20)$$

where $X(M, t_1, t_2)$ and $Y(M, t_1, t_2)$ are defined respectively as

$$X(M, t_1, t_2) \equiv \frac{\sigma^2(2M)[\delta_{c1} - 2\delta_{c2}] + \sigma^2(M)\delta_{c2}}{\sqrt{2\sigma^2(M)\sigma^2(2M)[\sigma^2(M) - \sigma^2(2M)]}}, \quad (21)$$

and

$$Y(M, t_1, t_2) \equiv \frac{\sigma^2(M)\delta_{c2} - \sigma^2(2M)\delta_{c1}}{\sqrt{2\sigma^2(M)\sigma^2(2M)[\sigma^2(M) - \sigma^2(2M)]}}. \quad (22)$$

Using the above formulae and equation (15), we write down the number density of bound systems which form with mass $M \sim M + dM$ at time $t_f \sim t_f + dt_f$ and survive without destroyed until later time t as

$$\begin{aligned} F(M, t_f, t) dM dt_f &\equiv R_{\text{form}}(M, t_f) dM dt_f \times P_{\text{surv}}(M, t_f, t) \\ &= \frac{1}{\sqrt{2\pi}} \frac{1}{\sqrt{\sigma^2(M/2) - \sigma^2(M)}} \left[2 - \left(\frac{\delta_c(t_f) - 2\delta_c(t)}{\delta_c(t)} \right) \right] \\ &\times \exp\left(\frac{2\delta_c(t)[\delta_c(t_f) - \delta_c(t)]}{\sigma^2(M)} \right) \text{erfc}[X(M, t_f, t)] \\ &- \text{erfc}[Y(M, t_f, t)] \left[-\frac{d\delta_c}{dt}(t_f) \right] N_{\text{PS}}(M, t_f) dM dt_f. \end{aligned} \quad (23)$$

Given a mass M and time t , equation (23) is regarded as the distribution function of formation epoch t_f . In Fig. 3 we plot $F(M, z_f, z = 0)$ versus z_f for several masses in the standard CDM model. A common feature is that F as a function of z_f remains nearly constant up to a certain redshift and

then starts to decline. The epoch at which F drops by an order of magnitude is $z_f \approx 6$ for $M = 10^9 M_\odot$, $z_f \approx 4$ for $M = 10^{11} M_\odot$, $z_f \approx 2$ for $M = 10^{13} M_\odot$, and $z_f \approx 0.6$ for $M = 10^{15} M_\odot$. These are interpreted as typical epochs for the formation of bound systems of respective masses which exist at $z = 0$.

3 X-RAY BACKGROUND RADIATION CONTRIBUTED FROM CLUSTERS OF GALAXIES

As a simple and important application of our formulae, we calculate X-ray emission from clusters of galaxies and their contribution to the observed XRB. The formation rate of virialized systems plays an essential role in specifying the epoch of formation of clusters and in explicitly taking account of their luminosity evolution.

3.1 Method of calculation

3.1.1 Cluster contribution to the XRB spectra

Clusters of galaxies are filled with diffuse hot plasma which produces copious X-ray emission. If the total power liberated per unit comoving volume and unit frequency at redshift z is denoted by $J_\nu(z)$, the background X-ray intensity I_{ν_0} observed at present at frequency ν_0 is described as

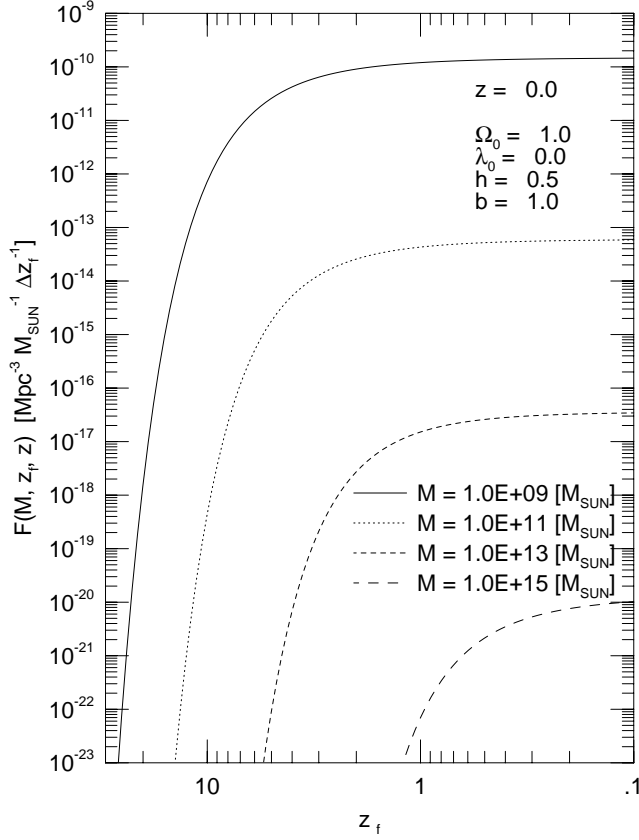


Figure 3. Distribution of formation epoch $F(M, z_f, z)$ in the standard CDM model. The differential number densities of bound objects that are formed at redshift z_f and survive until $z = 0$ are plotted against z_f for masses $M = 10^9 M_\odot$ (solid curve), $10^{11} M_\odot$ (dotted), $10^{13} M_\odot$ (short-dashed) and $10^{15} M_\odot$ (long-dashed).

$$I_{\nu_0} = \frac{c}{4\pi H_0} \int_0^\infty \frac{J_{\nu_0(1+z)}(z) dz}{(1+z)\sqrt{(\Omega_0 z + 1)(1+z)^2 - \lambda_0 z(2+z)}}, \quad (24)$$

where c is the speed of light, and λ_0 is the dimensionless cosmological constant. In our model, the luminosity at frequency ν of a cluster, $L_\nu(M, z_f, z)$, is assumed to be determined by the mass M , the epoch of its formation z_f , and the epoch z at which the observed X-ray is emitted (see eq.[34] below). Then $J_\nu(z)$ is given by

$$J_\nu(z) = \int_0^\infty dM \int_z^\infty dz_f F(M, z_f, z) L_\nu(M, z_f, z), \quad (25)$$

where $F(M, z_f, z)$ is the formation epoch distribution (eq. [23]).

In contrast to equation (25), previous authors calculated $J_\nu(z)$ using the mass function of clusters directly as follows (Evrard & Henry 1991; Blanchard et al. 1992; Burg et al 1993):

$$J_\nu(z) = \int_0^\infty dM N(M, z) L_\nu(M, z_f = z, z), \quad (26)$$

where the mass function $N(M, z)$ is often taken as the PS formula (eq. [1]). Since the mass function does not specify the epoch of formation of virialized clusters, z_f is usually set to be equal to the epoch of emission z . Such a treatment, however, is strictly justified only if z_f is very close to

z , and will become inappropriate otherwise. The properties of a virialized system such as radius and temperature are determined by z_f not z (see Section 3.1.2). Thus the luminosity evolution described in equation (26) is not realistic. In fact one frequently encounters similar situations where the formation epoch is essential in incorporating the evolution of individual astronomical objects and making cosmological predictions. This is one of the strong advantages of our current refinement of the original PS theory.

3.1.2 X-ray emission from clusters

The total gravitating mass of clusters is dominated by dissipationless dark matter, which is likely to be relaxed immediately after the collapse of halo and attain the virial equilibrium. In a theoretical treatment for the collapse of spherical perturbations, the radius of a virialized cluster in the Einstein-de Sitter ($\Omega_0 = 1$) universe is estimated as a half of maximum turn-around radius and given by

$$\begin{aligned} r_{\text{vir}} &= \frac{(GM)^{1/3}}{(3\pi H_0)^{2/3}} \frac{1}{1+z_f} \\ &= 1.69(1+z_f)^{-1} \left(\frac{M}{10^{15} M_\odot} \right)^{1/3} h^{-2/3} \text{ Mpc}, \quad (27) \end{aligned}$$

where M is the total mass of the cluster, and z_f is the redshift of its formation. The virial temperature of the system T_{vir} is then calculated as

$$\begin{aligned} T_{\text{vir}} &= \frac{GM\mu m_p}{3k_B r_{\text{vir}}} \\ &= 6.06 \times 10^7 \left(\frac{\mu}{0.59} \right) (1+z_f) \left(\frac{M}{10^{15} M_\odot} \right)^{2/3} h^{-2/3} \text{ K}, \quad (28) \end{aligned}$$

where G is the gravitational constant, k_B is the Boltzmann constant, m_p is the proton mass, and μ is the mean molecular weight. The cases of $\Omega_0 < 1$ universes are discussed in Appendix A. Hereafter we assume that the intracluster gas is fully ionized with the primordial abundance $Y = 0.24$, where Y is the helium fraction by weight, and thus $\mu = 0.59$. Note that once a model for the background universe is specified, properties of virialized clusters are determined by two parameters; mass M and the formation epoch z_f which is not available in the conventional PS theory.

The gas component of clusters generates the X-ray continuum emission mainly due to thermal bremsstrahlung whose emissivity in CGS units is (e.g., Rybicki & Lightman 1979)

$$\begin{aligned} \epsilon_\nu^{\text{ff}} &= 6.84 \times 10^{-38} \left(\frac{2}{2-Y} \right) \bar{g}(T_{\text{gas}}, \nu) \\ &\quad \times n_e^2 T_{\text{gas}}^{-1/2} \exp\left(-\frac{h\nu}{k_B T_{\text{gas}}}\right) \text{ erg s}^{-1} \text{ cm}^{-3} \text{ Hz}^{-1} \quad (29) \end{aligned}$$

where h is the Planck constant, T_{gas} is the gas temperature, and n_e is the electron density. We adopted an approximation $\bar{g}(T, \nu) = 0.9(h\nu/k_B T)^{-0.3}$ for the velocity-averaged Gaunt factor following Evrard & Henry (1991).

The X-ray emission described by equation (29) is essentially determined by the temperature and density profiles of intracluster gas. Simple models for the intracluster gas often assume that the gas is isothermal and its distribution is spherically symmetric. The observed X-ray

spectra and galaxy velocity dispersions further suggest that $T_{\text{vir}}/T_{\text{gas}} \approx 1$ (Mushotzky 1984). Thus we set

$$T_{\text{gas}} = T_{\text{vir}}(M, z_f). \quad (30)$$

For the density profile, the observed X-ray image of surface brightness is found to agree well with (Jones & Forman 1984)

$$\rho_{\text{gas}}(r) = \rho_{\text{gas}}^0 \left[1 + \left(\frac{r}{r_c} \right)^2 \right]^{-1}, \quad (31)$$

where ρ_{gas}^0 is the central gas density, r is the distance from the cluster centre, and r_c is the core radius. The above modeling is slightly different from the conventional isothermal β -model, in which the temperature and density profiles of intracluster gas are described by a single parameter β . Although our parametrization seems inconsistent with the β model, it can be reconciled if the galaxy number density scales as $[1 + (r/r_c)^2]^{-1}$ unlike the King model $[1 + (r/r_c)^2]^{-3/2}$. In fact, this is qualitatively indicated from some observations (Bahcall & Lubin 1994).

As for the core radius r_c , we still lack understandings of its physical meaning, and are unable to predict how it depends on M and z_f . Thus we adopt a simple self-similar model in which r_c is proportional to r_{vir} :

$$\begin{aligned} r_c &= 0.15h^{-1}\text{Mpc} \times \frac{r_{\text{vir}}(M, z_f)}{r_{\text{vir}}(10^{15}M_{\odot}, z_f = 0)} \\ &= 0.15(1 + z_f)^{-1} \left(\frac{M}{10^{15}M_{\odot}} \right)^{1/3} h^{-1}\text{Mpc}, \end{aligned} \quad (32)$$

where the normalization is chosen to match the *Ginga* observations (Hatsukade 1989), and the second equality assumes the Einstein-de Sitter universe. Then the central gas density ρ_{gas}^0 is fixed by

$$\int_0^{r_{\text{vir}}} \rho_{\text{gas}}(r) 4\pi r^2 dr = M \left(\frac{\Omega_B}{\Omega_0} \right), \quad (33)$$

where Ω_B is the baryonic density parameter.

In order to describe realistic X-ray emission from clusters, we also need to take account of intrinsic luminosity evolution. As the effects of merger are already factored out in equation (25), quiet gas accretion and the subsequent changes in temperature and density profiles are here to be incorporated. These processes, however, are still highly uncertain. So we attempt to model their effects into a factor $\gamma(z_f, z)$ and express the luminosity as

$$L_{\nu}(M, z_f, z) = \gamma(z_f, z) \int_0^{r_{\text{vir}}} \epsilon_{\nu}^{\text{ff}}(M, z_f; r) 4\pi r^2 dr, \quad (34)$$

where $L_{\nu}(M, z_f, z)$ is the luminosity that a cluster formed with mass M at redshift z_f would have at a later epoch z . Given a large degree of uncertainty, $\gamma(z_f, z)$ is assumed here to take a power law form:

$$\gamma(z_f, z) = \left(\frac{1 + z_f}{1 + z} \right)^p. \quad (35)$$

Current numerical simulations seem to indicate $p \lesssim 1$ (e.g., Evrard 1990; Sugimotohara 1995; Navarro, Frenk & White 1995), and we examine two limiting cases of no intrinsic evolution, $p = 0$, and of very strong evolution, $p = 1$.

Integrating equation (34) over whole frequency, one finds a simple scaling law for the bolometric luminosity of the form:

$$L_{\text{bol}}(M, z_f, z) \propto M^{4/3} (1 + z_f)^{q+p} (1 + z)^{-p}, \quad (36)$$

where the parameter q is constant and equal to $7/2$ in the Einstein-de Sitter universe, while it varies with z_f and less than $7/2$ in low Ω_0 universes; e.g. $1.8 \lesssim q \lesssim 3.5$ for $\Omega_0 = 0.2$ and $\lambda_0 = 0.8$.

3.1.3 X-ray temperature and luminosity functions

In Section 3.1.1, we have emphasized the difference between our formulation and the conventional PS approach. For more direct comparison of these two procedures, we also calculate the X-ray temperature and luminosity functions of clusters of galaxies.

In our model, the X-ray temperature function at redshift z is expressed using equation (23) as

$$N_{\text{T}}(T, z) dT = \int_z^{\infty} dz_f F(M, z_f, z) \frac{dM}{dT} \Big|_{M=M(T, z_f)} dT, \quad (37)$$

where $M(T, z_f)$ stands for the mass which gives the gas temperature T if formed at redshift z_f (e.g., eq. [28]). Here we have neglected the intrinsic evolution of gas temperature. On the other hand, from the PS mass function, one obtains

$$N_{\text{T}}(T, z) dT = N_{\text{PS}}(M, z) \frac{dM}{dT} \Big|_{M=M(T, z_f=z)} dT. \quad (38)$$

Note that z_f is set to be equal to z in the above equation.

Similarly, the X-ray luminosity function at redshift z in each approach is

$$N_{\text{L}}(L, z) dL = \int_z^{\infty} dz_f F(M, z_f, z) \frac{dM}{dL} \Big|_{M=M(L, z_f, z)} dL, \quad (39)$$

and

$$N_{\text{L}}(L, z) dL = N_{\text{PS}}(M, z) \frac{dM}{dL} \Big|_{M=M(L, z_f=z, z)} dL, \quad (40)$$

where $M(L, z_f, z)$ is solved from the integral of equation (34) over frequency.

3.2 Comparison with hydrodynamical simulation

It is meaningful to check the validity and limitations of our modeling through the comparison with other classes of approach. Fortunately a series of three-dimensional hydrodynamic simulations in a CDM model universe have been developed to study the evolution of X-ray clusters (Cen et al. 1990; Cen & Ostriker 1992, 1993, 1994; Kang et al. 1994; Bryan et al. 1994). In this subsection, therefore, we compare the results of our analytical approach with those of numerical simulations.

Figure 4 illustrates the temperature functions evaluated analytically by equations (37) and (38) respectively, in comparison with the results of the simulation by Kang et al. (1994) and the observations (Henry & Arnaud 1991). The cosmological parameters are the same as in Kang et al. (1994); $\Omega_0 = 1$, $h = 0.5$, $\Omega_B = 0.06$ and $b = 0.95$. The indicated error bars of the simulation data correspond to statistical ones only. The simulation data are kindly provided by Renyue Cen, and note that the original plots in Figures 1 to 5 of Kang et al. (1994) should be shifted down by a factor of $\ln 10$ due to an error in their plotting procedure (Cen, private communication).

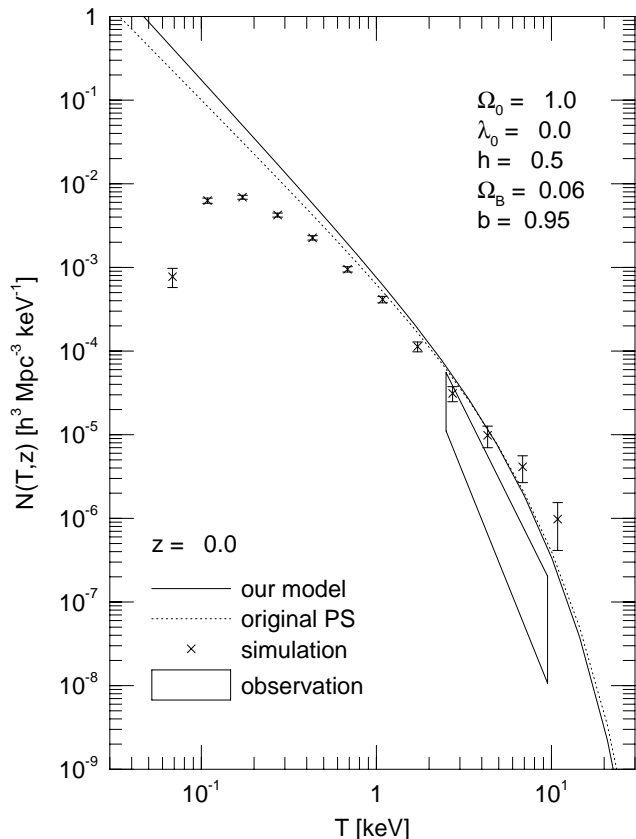


Figure 4. X-ray cluster temperature functions at redshift $z = 0$ in the CDM model; predictions of our model (eq. [37]) (solid curve), of the PS approach (eq. [38]) (dotted curve), and of the simulation by Kang et al. (1994) (crosses). The cosmological parameters are fixed in each as $\Omega_0 = 1$, $h = 0.5$, $\Omega_B = 0.06$ and $b = 0.95$. The error bars of the simulation data only indicate the statistical error. The squared region shows the error box of observations (Henry & Arnaud 1991).

The analytical results in Fig. 4 show a reasonable agreement with that of the numerical simulation above $T \sim 1$ keV. In fact, the simulation data are subject to much larger error below this temperature due to its spatial resolution of $\sim 0.75h^{-1}$ Mpc (Kang et al. 1994). They are also likely to be affected by the limited sample volume size at $T \gtrsim 10$ keV. The difference between our method and the previous PS approach is in general rather insignificant in this figure, because the temperature of a virialized system depends only weakly on z_f as $\propto (1 + z_f)$ in the $\Omega_0 = 1$ universe (eq. [28]). Such a feature is especially apparent at high temperatures, where most clusters that contribute are large and formed only at low redshifts. The difference becomes relatively larger at low temperatures where small clusters make dominant contributions.

The results for the bolometric luminosity functions are plotted in Fig. 5. Neither the simulation nor our analytical approach takes account of physical cooling or heating. This is justified in discussing the overall properties of clusters of galaxies except at the core. In contrast to Fig. 4, the difference between our method and the conventional PS approach is more significant, because the bolometric luminosity depends much more strongly on z_f as $\propto (1 + z_f)^{7/2}$

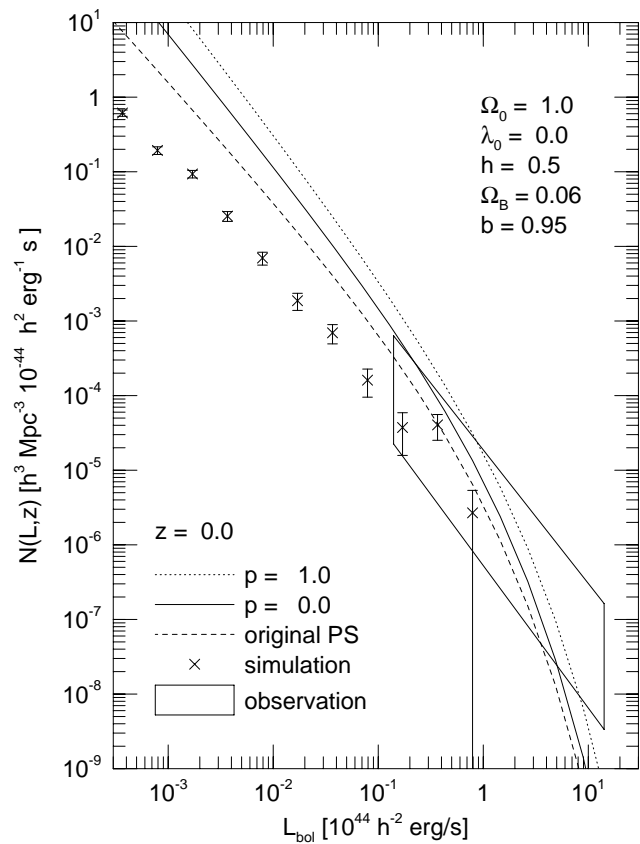


Figure 5. X-ray cluster bolometric luminosity functions at redshift $z = 0$ in the CDM model; predictions of our model (eq. [37]) with the parameter $p = 0$ (solid curve) and $p = 1$ (dotted curve), of the PS formalism (eq. [38]) (dashed curve), and of the simulation by Kang et al. (1994) (crosses). The cosmological parameters are the same as in Fig. 4. The error bars of the simulation data are only statistical. The squared region shows the error box of observations (Henry & Arnaud 1991).

(eq. [36]). The deviations from the simulation data are also larger and our changes to the PS formalism does not reconcile the discrepancy. However, as remarked by Cen (1992) and Kang et al. (1994), the numerical procedures tend to systematically underestimate the predicted luminosity, perhaps by a factor of ~ 2 . The underestimation would be severer at low luminosities where the effects of the spatial resolution becomes more important. In addition, the simulation clearly lacks the sample volume size for the statistically reliable predictions at $L_X \gtrsim 10^{44} h^{-2} \text{erg/s}$ where most of the observed data are available (Henry & Arnaud 1991). Thus the analytical results are not only qualitatively consistent with the numerical simulation, but also applicable in much wider dynamical range.

Figure 6 shows the predictions of the XRB spectra, together with the *ASCA* observations. The analytical results agree well with the simulation around $E \sim 10$ keV but predict larger intensity at $E \lesssim 2$ keV. This is reasonable if one considers the numerical effects including the spatial resolution of the simulation. As expected from the features in Fig. 5, our model systematically predicts higher intensity than the original PS formalism, and the intensity increases

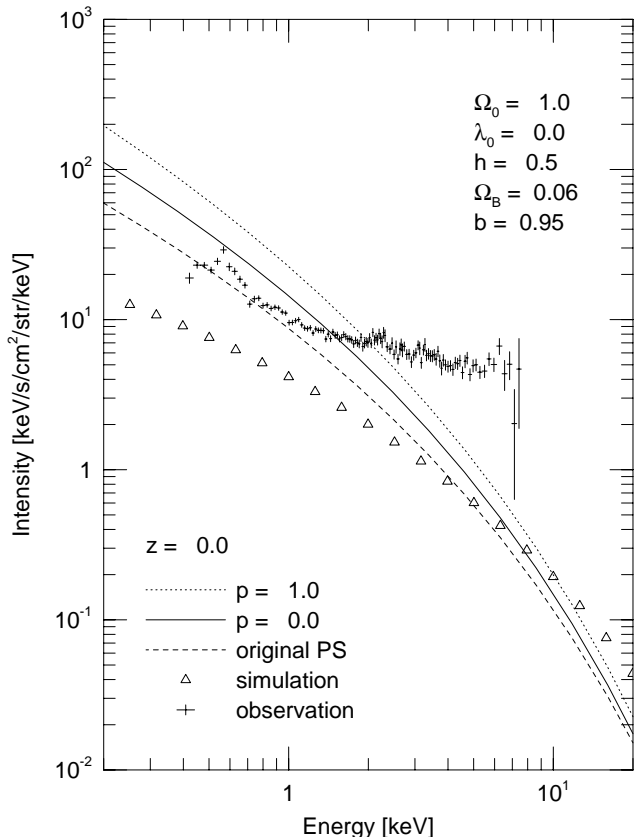


Figure 6. The XRB spectra contributed from clusters of galaxies; predictions of our model (eq. [25]) with the parameter $p = 0$ (solid curve) and $p = 1$ (dotted curve), of the PS formalism (eq. [26]) (dashed curve), and of the simulation by Kang et al. (1994) (triangles). The cosmological parameters are the same as in Fig. 4. Also plotted are the observed data from *ASCA* with statistical errors (Gendreau et al. 1994).

as the intrinsic evolution indicated by the parameter p becomes stronger.

As a matter of fact, our method and numerical simulations are complementary to each other in predicting the X-ray properties of clusters and their contribution to the XRB spectra. The analytical approach basically has two advantages; one is that it is much easier to make systematic parameter surveys. Therefore it would give a better insight into how the predictions depend on the distribution of intra-cluster gas, the luminosity evolution, and the geometry of the background universe. The other is that the results are largely free from the small-scale resolution or the limited volume size that may affect the numerical results. Alternatively, our present predictions do not properly take account of the thermal evolution of clusters induced by the interaction between gas and radiation, which will be incorporated in due course. In addition, we have assumed a rather simplified gas density profile as well as a spherical distribution of dark matter.

Table 1. Models for the background universe

Model	Ω_0	λ_0	h	Ω_B	b
E5	1	0	0.5	0.05	0.71
E8	1	0	0.8	0.02	0.43
O5	0.2	0	0.5	0.05	6.7
O8	0.2	0	0.8	0.02	2.8
L5	0.2	0.8	0.5	0.05	2.2
L8	0.2	0.8	0.8	0.02	1.0

3.3 Predictions for various cosmological models

In this subsection, we present the XRB spectra to constrain the viable sets of cosmological parameters in a CDM universe. Specifically we consider six CDM models listed in Table 1. Values of the Hubble parameter h are taken as either 0.5 or 0.8, where the latter is strongly motivated from the observation of Cepheids in the Virgo cluster by the Hubble Space Telescope (Freedman et al. 1994). In each model, the baryon density of the universe is assumed to be $\Omega_B h^2 = 0.0125$, which is consistent with primordial nucleosynthesis (e.g., Walker et al. 1991). The biasing parameter b is given by normalizing the amplitude of the fluctuation spectrum by the *COBE* DMR two year data (Sugiyama 1995). The critical overdensity for the spherical collapse δ_c is taken as $\delta_c = 1.69$ in models E5, E8, L5 and L8, and $\delta_c = 1.64$ in O5 and O8 (Lilje 1992; LC).

Figures 7, 8 and 9 illustrate the calculated XRB spectra together with the *ASCA* observations (Gendreau et al. 1994). There are a few points that need to be kept in mind. Firstly, line emissions or absorptions from metals are omitted in our calculation. This may lead to underestimation of XRB intensity below 1 keV (Cen et al. 1995). Secondly, a steep rise in the observed intensity in the soft X-ray band may be partly due to Galactic emission (McCammon & Sanders 1990; Snowden et al. 1990). Finally, it has been suggested from the high-resolution image of *ROSAT* that at least 30% of the XRB at 1 keV is contributed from quasars (Shanks et al. 1991).

Having considered the above points, we see that models E5 and E8 overproduce the soft X-ray intensity (Fig. 7). While this result was pointed out earlier by Burg et al. (1993) on the basis of the conventional PS approach, such a feature is more apparent in our model which takes account of the formation rate. The overproduction could be removed if the clusters underwent considerable *anti-evolution* against the growth of the gravitational potential (Burg et al. 1993). Alternative ways to avoid such discrepancy are to consider a small value for the Hubble constant; e.g., $h \lesssim 0.3$, or to abandon the *COBE* normalization and introduce much smaller fluctuation amplitude, both of which are highly artificial even if not completely excluded. Therefore the $\Omega_0 = 1$ CDM universes have a serious difficulty of overproducing the XRB.

On the other hand, Fig. 8 shows that the predicted intensity in models O5 and O8 is significantly smaller and that clusters of galaxies do not basically contribute to the XRB in these models. As a matter of fact, this is mainly because of large values of the biasing parameter b imposed from the *COBE* data. Clusters of galaxies are thus rejected as a candidate for the origin of the XRB in these open models.

Noticeably, Fig. 9 suggests that the observed XRB at

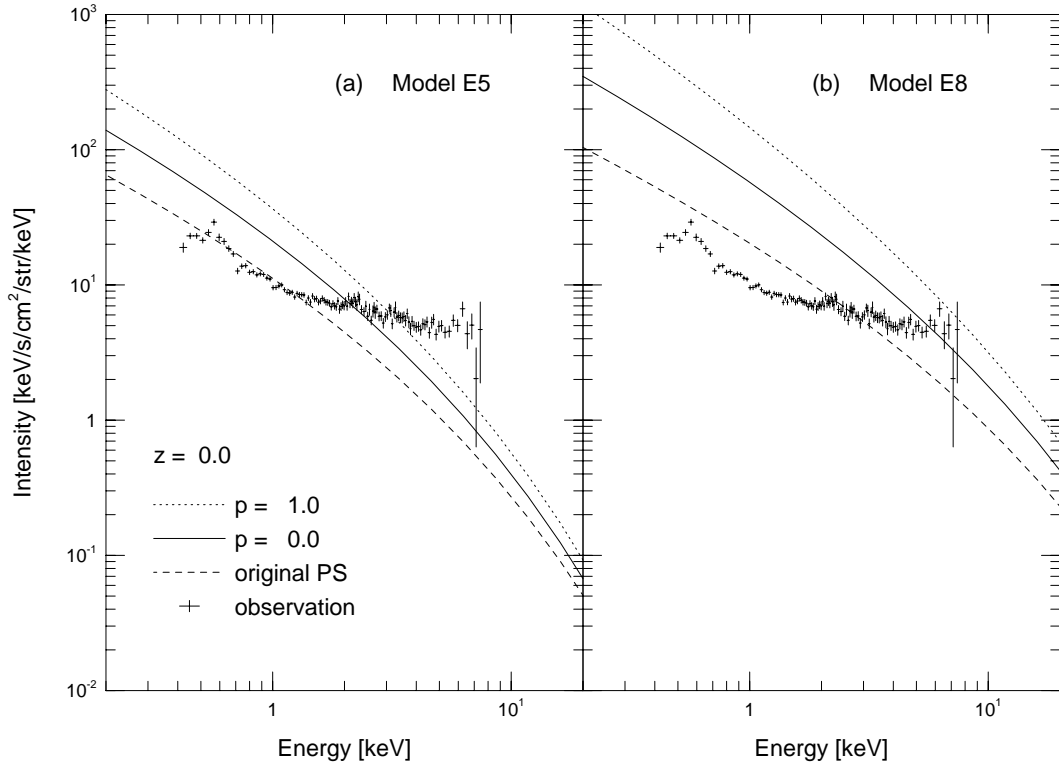


Figure 7. The XRB spectra contributed by clusters of galaxies in the Einstein-de Sitter universe; (a) E5, (b) E8. Lines show predictions of our model with the parameter $p = 0$ (solid) and $p = 1$ (dotted), and of the original PS formalism (dashed). Also plotted are the *ASCA* observations from Gendreau et al. (1994).

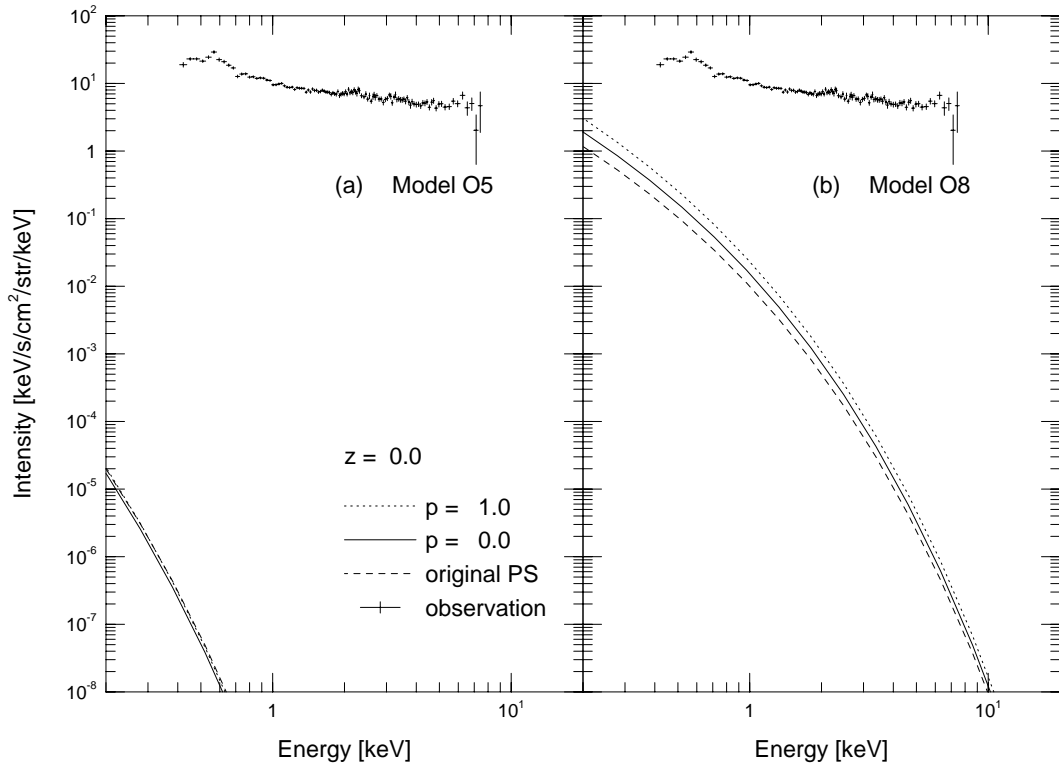


Figure 8. Same as in Fig. 7 except that the background universe is open ($\Omega_0 = 0.2$, $\lambda_0 = 0$); (a) O5, (b) O8.

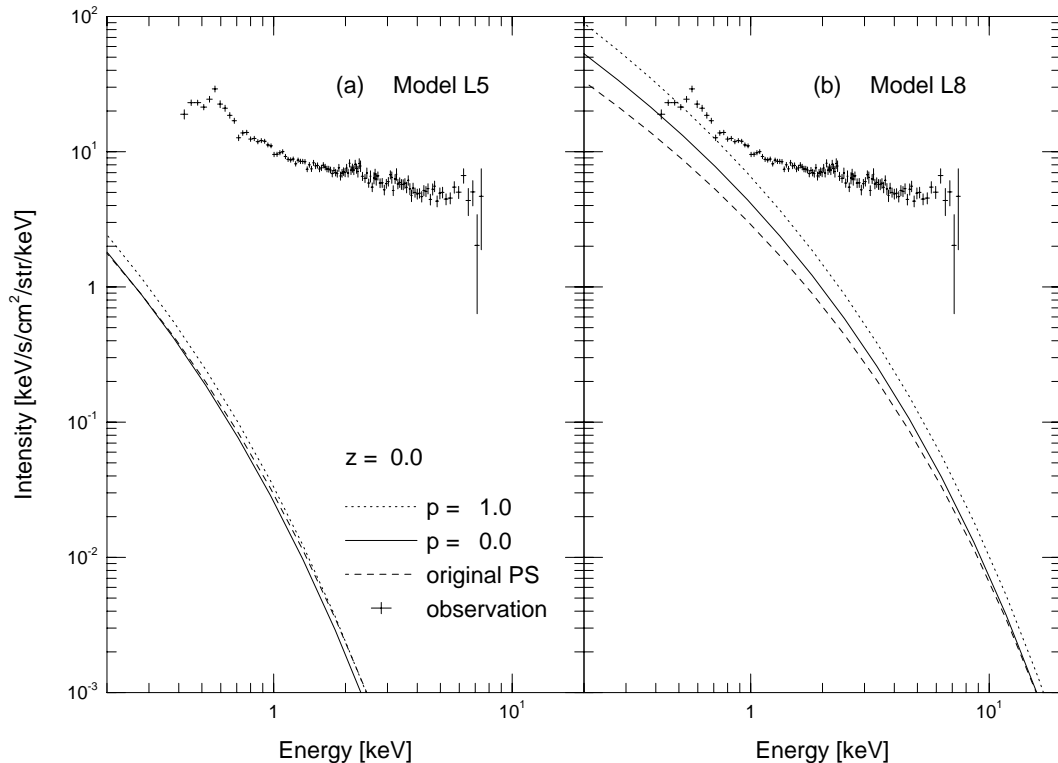


Figure 9. Same as in Fig. 7 except that the background universe is spatially flat with the cosmological constant ($\Omega_0 = 0.2$, $\lambda_0 = 0.8$); (a) L5, (b) L8.

$E \lesssim 0.8\text{keV}$ attains a dominant contribution from clusters of galaxies in model L8. We should, however, be careful because the observation in this band is most sensitive to the contamination due to Galactic absorptions and emissions. Nevertheless it is interesting to see a possibility that a part of the XRB can be naturally explained by clusters of galaxies in one of promising cosmological models.

4 CONCLUSIONS

We have extended the theory of Press & Schechter (1974) and the formulation of Bower (1991) and Lacey & Cole (1993) to derive expressions for the rates of formation and destruction of gravitationally bound systems. Although the formal expressions of these quantities diverge, they properly reproduce the time derivative of the PS mass function. The divergence is not unphysical but can be interpreted as being originated from the somewhat improper definition of formation and destruction of bound objects. We have proposed a phenomenological prescription to remove such divergences by specifying a realistic mass range in which the identity of an object is to be maintained. The resulting expressions are practically insensitive to the choice of the threshold masses. On the basis of this prescription, we have obtained a distribution function of formation epochs of bound systems. This quantity is of great cosmological importance because it provides a useful theoretical tool in describing the subsequent evolution of the systems.

In order to exhibit the applicability of the above formalism, we have evaluated the contribution of clusters of galax-

ies to the XRB, as well as the X-ray cluster temperature and luminosity functions. Changes from the previous PS formalism are obvious especially when the cluster evolution is strong and the X-ray properties depend largely on its formation epoch. The results of our analytical procedure, although fairly phenomenological in modelling clusters' X-ray gas, are reasonably supported by those of the three-dimensional hydrodynamical simulation by Kang et al. (1994). Thus these two approaches are complementary in investigating the evolution history of virialized structures.

We have shown that the significant fraction of the observed soft XRB can be accounted for by clusters of galaxies in a spatially flat CDM universe with $\Omega_0 \sim 0.2$ and $\lambda_0 = 1 - \Omega_0$ with the *COBE* DMR two year normalization. The $\Omega_0 = 1$ CDM model tends to overproduce the observed X-ray intensity. On the other hand, the cluster contribution becomes negligibly small in an open CDM universe with $\Omega_0 \sim 0.2$, in which case observed XRB should be explained entirely by other classes of sources such as quasars. Although our overall conclusion in the $\Omega_0 = 1$ case agrees with Burg et al. (1993), we derived new constraints on the other models from the XRB in a consistent and clear manner. Note that the model with $\Omega_0 \sim 0.2$, $\lambda_0 = 1 - \Omega_0$ and $h \sim 0.8$ is a specific example of the most successful cosmological models explaining the cosmic age, two-point correlation functions of galaxies and clusters, and small-scale velocity dispersions (Efstathiou et al. 1990; Sugimotohara & Suto 1991; Suto 1993; Watanabe, Matsubara & Suto 1994; Bahcall 1994). In this context it is interesting to note that the same model can simultaneously account for a major fraction of the observed

XRB in the soft energy band. Furthermore, the microwave background distortion and the resulting anisotropy due to the distant clusters in CDM models are below the current limit (Makino & Suto 1993).

Obviously there remain several areas for further theoretical work. With regard to the XRB predictions, the greatest uncertainty probably lies in the evolution of intracluster medium. Although we have assumed that it basically traces the growth of the gravitational potential, this assumption is still an open question and different evolutionary models would alter the predicted luminosity functions and the XRB spectra. The contamination of the observed spectra by the Galactic emission and absorption is also uncertain. Moreover, we have omitted the line emissions which may affect the soft band intensity. Therefore we did not aim to rigorously reproduce the XRB spectra from theory, but rather to examine the possibility that clusters of galaxies play a crucial role in the origin of the XRB.

As to the formalism, on the other hand, our method contains a formal divergence for which somewhat artificial prescription has been proposed. In addition, our argument itself has further room for improvement; for instance, if M_1 in equation (13) does not correspond to the largest parent of the final object M , the rate of formation thereby defined possibly overcounts the true rate. This problem is in fact ascribed to a fundamental limitation of the current formalism which does not take into account the history of every single object involved in a merger process. Clearly the validity of our treatment needs to be examined through a direct comparison with other classes of approach such as N-body simulations. Other ways of formulation are also desirable. In this context we note that LC proposed a differential distribution function of halo formation times based on what they called ‘the halo counting argument’ (see their §2.5.2). As notified by LC, however, their definition leads to a slight self-inconsistency of predicting a negative probability density depending on the slope of the fluctuation spectrum. As a matter of fact, we compared their result with ours and basically confirmed that both agree well in the mass range of astrophysical interest. For practical purposes, therefore, our present formulae are expected to be applicable to a number of further problems in cosmology such as cluster luminosity functions in various cosmological models, formation of high redshift objects and reionization history of the universe. These issues, together with a quantitative comparison with LC, will be described elsewhere (Kitayama & Suto, in preparation).

ACKNOWLEDGEMENTS

We thank Shin Sasaki, Katsuhiko Sato, Tatsushi Sugihara, Hajime Susa, and Takahiro Tanaka for helpful discussions and comments. We are grateful to Renyue Cen, Keith Gendreau and Naoshi Sugiyama for providing the relevant results of their current work which are adopted in the present paper. TK acknowledges the fellowship from the Nippon Telephone and Telegram Co. . This research is supported in part by the Grants-in-Aid by the Ministry of Education, Science and Culture of Japan (05640312, 06233209, 07740183, 07CE2002).

REFERENCES

- Bahcall N. A., 1994, preprint POP-606
 Bahcall N. A., Lubin L. M., 1994, *ApJ*, 426, 513
 Blain A. W., Longair M. S., 1993a, *MNRAS*, 264, 509
 Blain A. W., Longair M. S., 1993b, *MNRAS*, 265, L21
 Blanchard A., Wachter K., Evrard A. E., Silk J., 1992, *ApJ*, 391, 1
 Bond J. R., Cole S., Efstathiou G., Kaiser N., 1991, *ApJ*, 379, 440
 Bower R. J., 1991, *MNRAS*, 248, 332
 Bryan G. L., Cen R., Norman M. L., Ostriker J. P., Stone J. M., 1994, *ApJ*, 428, 405
 Burg R., Cavaliere A., Menci N., 1993, *ApJ*, 404, L55
 Cavaliere A., Colafrancesco S., Scaramella R., 1991, *ApJ*, 380, 15
 Cen R., 1992, *ApJS*, 78, 341
 Cen R., Jameson A., Liu F., Ostriker J. P., 1990, *ApJ*, 362, L41
 Cen R., Kang H., Ostriker J. P., Ryu D., 1995, submitted to *ApJ*
 Cen R., Ostriker J. P., 1992, *ApJ*, 393, 22
 Cen R., Ostriker J. P., 1993, *ApJ*, 417, 404
 Cen R., Ostriker J. P., 1994, *ApJ*, 429, 4
 Davis M., Efstathiou G., Frenk C., White S., 1985, *ApJ*, 292, 371
 Efstathiou G., Rees M. J., 1988, *MNRAS*, 230, 5p
 Efstathiou G., Sutherland W. J., Maddox S. J., 1990, *Nature*, 348, 705
 Evrard A. E., 1990, *ApJ*, 363, 349
 Evrard A. E., Henry J. P., 1991, *ApJ*, 383, 95
 Freedman et al. 1994, *Nature*, 371, 757
 Fukugita M., Kawasaki M., 1994, *MNRAS*, 269, 563
 Gendreau K. C., et al., 1994, in Makino F., Ohashi T., eds, *New Horizon of X-ray Astronomy – First Results from ASCA*. Universal Academy Press, Tokyo, p.365
 Hatsukade I., 1989, Osaka University PhD thesis (unpublished)
 Henry J. P., Arnaud K. A., 1991, *ApJ*, 372, 410
 Jones C., Forman W., 1984, *ApJ*, 276, 38
 Kang H., Cen R., Ostriker J. P., Ryu D., 1994, *ApJ*, 428, 1
 Kauffmann G., White S. D. M., 1993, *MNRAS*, 261, 921
 Lacey C. G., Cole S., 1993, *MNRAS*, 262, 627 (LC)
 Lahav O., Lilje P. B., Primack J. R., Rees M. J., 1991, *MNRAS*, 251, 128
 Lilje P. B., 1992, *ApJ*, 386, L33
 Makino N., Suto Y., 1993, *ApJ*, 405, 1
 McCammon D., Sanders W. T., 1990, *Annu. Rev. Astron. Astrophys.*, 1990, 28, 657
 Mushotzky R. F., 1984, *PhysScr*, T7, 157
 Navarro, J.F., Frenk, C.S., White, S.D.M., 1995, *MNRAS*, 275, 720
 Peebles P. J. E., 1980, *The Large-Scale Structure of the Universe*, Princeton Univ. Press, Princeton
 Press W. H., Schechter P., 1974, *ApJ*, 187, 425 (PS)
 Rybicki G. B., Lightman A. P., 1979, *Radiative Processes in Astrophysics*. Wiley, New York
 Sarazin C. L., 1988, *X-ray Emission from Clusters of Galaxies*. Cambridge Univ. Press, Cambridge
 Sasaki S., 1994, *PASJ*, 46, 427
 Sasaki S., Takahara F., 1994, 91, 699
 Sasaki S., Takahara F., Suto, Y., 1993, *Prog. Theor. Phys.*, 90, 85
 Schaeffer R., Silk J., 1988, *ApJ*, 332, 1
 Shanks T., Georgantopoulos I., Stewart G. C., Pounds K. A., Boyle B. J., Griffiths R. E., 1991, *Nature*, 353, 315
 Silk J., Tarter J., 1973, *ApJ*, 183, 387
 Snowden S. L., Cox D. P., McCammon D., Sanders W. T., 1990, *ApJ*, 354, 211
 Sugihara T., 1994, *PASJ*, 46, 441
 Sugihara T., 1995, personal communication
 Sugihara T., Suto Y., 1991, *PASJ*, 43, L17
 Sugiyama N., 1995, submitted to *ApJ*

- Suto Y., 1993, Prog.Theor.Phys., 90, 1173
 Walker T. P., et al., 1991, ApJ, 376, 51
 Watanabe T., Matsubara T., Suto Y. 1994, ApJ, 432, 17
 White S. D. M., Frenk C. S., 1991, ApJ, 379, 52

APPENDIX A: RADIUS OF VIRIALIZED CLUSTERS IN LOW Ω_0 UNIVERSES

In an open universe ($\Omega_0 < 1$, $\lambda_0 = 0$), the effective radius that a spherical perturbation attains when it virializes is estimated as half of its maximum radius at turn-around. If a virialized system is formed with mass M at redshift z_f , one can readily show that the radius r_{vir} is given by

$$r_{\text{vir}} = \frac{(GM)^{1/3}}{1 - \Omega_0} \left\{ \frac{\Omega_0(\sinh \eta_f - \eta_f)}{4\pi H_0} \right\}^{2/3} \quad (\text{A1})$$

where η_f is expressed in terms of the epoch of collapse z_f as

$$\eta_f = \text{arccosh} \left[\frac{2(1 - \Omega_0)}{\Omega_0(1 + z_f)} + 1 \right]. \quad (\text{A2})$$

In the presence of the cosmological constant λ_0 , the dynamical motion of a spherical perturbation is modified and the radius r_{vir} of a virialized cluster is no longer half of the turn-around radius r_{ta} . In fact, the ratio of these two quantities is shown to obey the following cubic equation (Lahav et al. 1991):

$$2\chi \left(\frac{r_{\text{vir}}}{r_{\text{ta}}} \right)^3 - (2 + \chi) \left(\frac{r_{\text{vir}}}{r_{\text{ta}}} \right) + 1 = 0, \quad (\text{A3})$$

where

$$\chi \equiv \frac{\lambda_0 H_0^2}{GM} r_{\text{ta}}^3. \quad (\text{A4})$$

The condition for a shell to turn around is $\chi < 1$. Lahav et al. (1991) found a following approximated solution to equation (A3):

$$\frac{r_{\text{vir}}}{r_{\text{ta}}} \approx \frac{2 - \chi}{4 - \chi}. \quad (\text{A5})$$

For $\lambda_0 = 0$, the above result reproduces $r_{\text{vir}}/r_{\text{ta}} = 1/2$.

Now the maximum turn-around radius r_{ta} is no longer expressed as a simple analytical form if λ_0 is nonzero. For our present purpose, however, we simply assume that the presence of λ_0 affects the dynamics of the perturbation only through equation (A3) and it does not alter the value of r_{ta} itself. Then in a spatially flat universe ($\Omega_0 < 1$, $\lambda = 1 - \Omega_0$) which we discussed in the present paper, r_{ta} is written down as

$$r_{\text{ta}} = 2(GM)^{1/3} \left(\frac{\zeta_f}{3\pi H_0 \sqrt{1 - \Omega_0}} \right)^{2/3}, \quad (\text{A6})$$

where ζ_f is related to z_f via

$$\zeta_f \equiv \text{arcsinh} \left[\sqrt{\left(\frac{1}{\Omega_0} - 1 \right) \frac{1}{(1 + z_f)^3}} \right]. \quad (\text{A7})$$